



Published in final edited form as:

Neuroimage. 2012 February 1; 59(3): 2073–2087. doi:10.1016/j.neuroimage.2011.10.042.

Statistical Feature Extraction for Artifact Removal from Concurrent fMRI-EEG Recordings

Zhongming Liu*, Jacco A. de Zwart, Peter van Gelderen, Li-Wei Kuo, and Jeff H. Duyn
Advanced MRI Section, Laboratory of Functional and Molecular Imaging, National Institute of Neurological Disorders and Stroke, National Institutes of Health, Bethesda, MD, USA

Abstract

We propose a set of algorithms for sequentially removing artifacts related to MRI gradient switching and cardiac pulsations from electroencephalography (EEG) data recorded during functional magnetic resonance imaging (fMRI). Special emphases are directed upon the use of statistical metrics and methods for the extraction and selection of features that characterize gradient and pulse artifacts. To remove gradient artifacts, we use a channel-wise filtering based on singular value decomposition (SVD). To remove pulse artifacts, we first decompose data into temporally independent components and then select a compact cluster of components that possess sustained high mutual information with the electrocardiogram (ECG). After the removal of these components, the time courses of remaining components are filtered by SVD to remove the temporal patterns phase-locked to the cardiac markers derived from the ECG. The filtered component time courses are then inversely transformed into multi-channel EEG time series free of pulse artifacts. Evaluation based on a large set of simultaneous EEG-fMRI data obtained during a variety of behavioral tasks, sensory stimulations and resting conditions showed excellent data quality and robust performance attainable by the proposed methods. These algorithms have been implemented as a Matlab-based toolbox made freely available for public access and research use.

Keywords

gradient artifact; ballistocardiogram; singular value decomposition; independent component analysis; mutual information

INTRODUCTION

In parallel with the growing interest in combining electrophysiological and hemodynamic measurements in functional neuroimaging, steady progress has been made in techniques for simultaneous recording of EEG and fMRI signals (He and Liu, 2008; Ritter and Villringer, 2006). During a concurrent fMRI-EEG experiment, EEG recordings are severely contaminated by artifacts caused by the electromotive force (EMF) induced in the conductive loops formed by the scalp electrodes and the finite inter-electrode impedance of the head (Goldman et al., 2000). Since the EMF is proportional to the changing rate of the magnetic flux, artifactual electrical voltages can be induced by rapid switching of magnetic field gradients and/or subtle motion of electrodes within the static magnetic field. The

*Correspondence Zhongming Liu, PhD, Advanced MRI Section, LFMI, NINDS, NIH, Building 10, Room B1D-723, 9000 Rockville Pike – MSC 1065, Bethesda, Maryland 20982-1065, Phone: +1 301 451 9915, Fax: +1 301 480 1981, liuz5@mail.nih.gov.

Publisher's Disclaimer: This is a PDF file of an unedited manuscript that has been accepted for publication. As a service to our customers we are providing this early version of the manuscript. The manuscript will undergo copyediting, typesetting, and review of the resulting proof before it is published in its final citable form. Please note that during the production process errors may be discovered which could affect the content, and all legal disclaimers that apply to the journal pertain.

former is referred to as the gradient artifact (GA); the latter is often called the ballistocardiographic (BCG) or pulse artifact (PA) because the pulsatile blood flow originating from the heart is the dominant source of electrode motion on the scalp surface (Debener et al., 2008; Huang-Hellinger et al., 1995; Yan et al., 2010). These artifacts can dominate and obscure neurogenic EEG signals and remain difficult to eliminate in real-time. Therefore, retrospective processing algorithms are being actively explored to remove these artifacts off-line in order to uncover brain signals from contaminated recordings (Laufs et al., 2008).

In a typical fMRI study using the blood oxygen level dependent (BOLD) contrast, a selected brain volume is scanned repeatedly and each volume consists of a number of separate slice acquisitions using a 2-D gradient-echo or spin-echo echo planar imaging (EPI) sequence. Since the same gradient waveform is applied every time when a new slice is acquired, the induced gradient artifacts in concurrent EEG recordings are highly repetitive and phase-locked to the onset time of each slice acquisition. For this reason most existing methods for removing gradient artifacts share a common strategy of subtracting (or regressing out) from the raw data a temporal template or a group of templates that collectively characterizes the reoccurring patterns at every acquisition, leaving out brain signals that are expected to be independent of the timing of fMRI scanning (Allen et al., 2000; Freyer et al., 2009; Mandelkowitz et al., 2010; Negishi et al., 2004; Niazy et al., 2005; Ryali et al., 2009; Sijbers et al., 1999; Wan et al., 2006). However, different ways to derive such artifact templates from recorded data can arrive at varying degrees of residual artifacts and a potential loss of neuroelectrical signals. The ideal GA removal approach needs to account for the variability of gradient artifact due to the misalignment of fMRI and EEG sampling clocks (Anami et al., 2003; Mandelkowitz et al., 2006), slow drift of magnetic field gradients (Grouiller et al., 2007; Laufs et al., 2008) and head motion (Moosmann et al., 2009), and to minimize the inclusion of other non-GA signals to avoid undesired removal of brain signals.

Similar to the gradient artifact, the pulse artifact also exhibits periodicity: a similar pulse artifact reoccurs following each heart beat. Depending on the field strength (Debener et al., 2008) and the electrode setting (Goldman et al., 2000), the pulse artifact has an amplitude typically 1~4 times as large as neurogenic EEG signals. Such reoccurring artifacts are thought to be driven by pulsatile blood flow and are time-locked to cardiac activity (Huang-Hellinger et al., 1995). As cardiac cycles can be monitored through ECG recorded simultaneously with the EEG, PA removal strategies have been based on template subtraction methods similar to those used for gradient artifact removal (Allen et al., 1998; Ellingson et al., 2004; Goldman et al., 2000; Niazy et al., 2005; Sijbers et al., 2000; Vincent et al., 2007). However, due to the much larger temporal variability of the pulse artifact relative to the gradient artifact, PA removal is often less complete. Cardiac activity consists of a chain of coupled electrical and mechanical processes, which may vary from beat to beat even in normal conditions. Furthermore, each bolus of blood pumped out of the heart needs to circulate through a complex path before reaching the head and affecting the EEG. A number of sources of temporal variability may exist along this path, causing the ensuing pulse artifacts to appear as spatially complex, temporally non-stationary and spectrally non-specific signals. These characteristics limit the efficacy of existing template subtraction methods and make pulse artifacts much more difficult to remove than gradient artifacts.

Alternative to template subtraction methods are blind source separation techniques such as independent component analysis (ICA), which has been proposed to separate pulse artifacts and brain signals in a data-driven manner. Application of ICA after gradient artifact removal generates a mixture of components with mutually independent temporal behaviors (Benar et al., 2003; Debener et al., 2007; Leclercq et al., 2009; Mantini et al., 2007; Nakamura et al., 2006; Srivastava et al., 2005; Vanderperren et al., 2010). Brain signals and pulse artifacts

arise from independent processes and thus are thought to comprise different independent components (IC). If one could attribute each IC to either a brain or PA-related source, a straight-forward data reconstruction (i.e. a reverse transformation of linear ICA) from only the non-PA components would produce artifact-free brain signals. Despite the conceptual simplicity of ICA, its usefulness for PA correction is to some extent compromised by the following theoretical and practical issues. The effectiveness of ICA-based signal-artifact separation depends on several factors such as which of the several available computational algorithms is used, on the statistical definitions of independence, on the number of components and the number of time points. Note that the underlying blood flow that causes the wide-spread electrode motion is such a complex and dynamic process that not only the amplitude but also the shape of the pulse artifact can vary substantially from electrode to electrode. It is rather difficult, if not impossible, to fully characterize the pulse artifact with just a few ICs. For this reason the pulse artifacts contribute to all components to different degrees. This is true especially when only a few electrodes or an insufficient number of temporal samples are available. Moreover, the number of artifactual components to remove is not a-priori known, and quantitative criteria for component selection are either lacking (Benar et al., 2003; Mantini et al., 2007; Nakamura et al., 2006) or problematic (Debener et al., 2007; Srivastava et al., 2005; Vanderperren et al., 2010). For instance, some groups have proposed to calculate the correlation between each component time-course and the recorded ECG and identify artifactual components by comparing their correlation coefficients to a rather low threshold (e.g. 0.2 or 0.15) (Debener et al., 2007; Srivastava et al., 2005; Vanderperren et al., 2010). However, because the time-courses of the pulse artifact and the ECG are highly dissimilar and have a complex and nonlinear relationship, this criterion cannot provide sufficient confidence or statistical power for component selection.

To effectively remove gradient and pulse artifacts, we ought to identify their characterizing features and accordingly define effective statistical metrics that allow for automatic and optimal signal-artifact separation. In contrast to previously published methods, we propose a set of algorithms, which extend from existing methods for statistical pattern recognition and classification (Jain et al., 2000), for the extraction and selection of artifactual features while MRI triggers and ECG serve as feature-defining variables. Once defined, these artifactual features can be subsequently removed from recorded data through regression analysis. The proposed algorithms have been used to process simultaneously acquired EEG-fMRI data with excellent performance for a large group of subjects with various experimental paradigms. As the scientific findings and group-level data analysis will be reported elsewhere, some examples from individual subject's data are provided here to demonstrate the usefulness of the proposed method in EEG artifact removal. In parallel with the publication of this article, a Matlab-based implementation of the algorithms described herein will be released for research use under the GNU general public license as open source code, accessible through <http://www.amri.ninds.nih.gov/software.html>.

METHODS AND MATERIALS

Simultaneous EEG-fMRI Acquisition

Twenty-five healthy human subjects (age 28 ± 10 , 13 female) participated in the study after giving informed written consent in accordance with a protocol approved by the Institutional Review Board at the National Institute of Neurological Disorders and Stroke. We acquired concurrent EEG/ECG (31-channel EEG, international 10–20 montage, one unipolar ECG, 16-bit BrainAmp MR, BrainProducts GmbH, Germany) and BOLD fMRI (GE-EPI, rate-2 SENSE, flip angle=90°, TE=30 ms, TR=1.5 or 2.1s, thirty 4 mm axial slices, FOV=220×165 mm², matrix size=64×48) using a GE 3-T Signa scanner equipped with a 16-channel receive-only coil array (Nova Medical, Wakefield, MA, USA). Continuous EEG and ECG data were referenced to the FCz electrode and sampled at 5 kHz with a resolution of 0.5μV/

bit and an analog bandwidth from 0.1 to 250Hz. The EEG sampling clock was synchronized with an external reference signal obtained from the 10MHz master clock of the MRI scanner. A slice-trigger signal that marked the onset time of every fMRI slice acquisition was also recorded based on a 5V TTL signal from the scanner. The fMRI acquisition was evenly spaced with equal delay between each excitation.

Experimental Paradigms

All subjects were instructed to lie inside the scanner in a dark environment. Each subject underwent multiple recording sessions with resting, behavioral, motor and sensory stimulation paradigms. As detailed experimental design and protocol will be described elsewhere, the data presented here were obtained from the paradigms briefly described as follows. In a resting experiment, the subject was instructed to relax for 10 minutes with eyes closed; in an eyes-closed-eyes-open task, the subject rested for 4 minutes with multiple cycles of self-paced alternating eyes-closed or eyes-open periods of about 30s each (volunteers marked changes between states by a button press); in a visual stimulation paradigm, the subject performed a fixation task while a full-field checkerboard was reversed at 2, 6 or 10Hz using a block design with three 30s stimulus-on periods interleaving four 30s fixation-only control periods.

From one subject, we also collected two 10-min datasets in the absence of gradient switching. One set was acquired when the subject sat quietly with eyes closed in the control room and the second set when the volunteer laid inside the MRI scanner without EPI acquisition. These two recording environments provided “clean” data to which the simultaneous EEG-fMRI data after the proposed artifact correction were compared.

From another subject, we recorded visual evoked potentials (VEP) and task-induced alpha modulation in a patient preparation room without magnetic interference, as well as inside the MRI scanner during concurrent fMRI scanning. The former provided reference signals for the assessment of artifact correction methods applied to the latter. The environment for recording outside the scanner was made as similar as possible to that inside the scanner. This entailed the volunteer being in the supine position inside the head coil, the front-projection mirror mounted on the coil, the projection screen as well as the use of a similar DLP projector and closely matched field of view. For VEP, 2-Hz full-field visual stimuli were presented with a block design; for the alpha modulation, the subject voluntarily opened and closed her eyes about every 30 seconds.

Gradient Artifact Removal

We developed an algorithm to remove the gradient artifact channel by channel. The raw data recorded from each channel were divided into epochs according to the fMRI slice trigger timing: one epoch was defined as the data acquired during the interval between one slice trigger and the next. After removing the mean of each epoch, all the epochs were arranged into a data matrix $\mathbf{D}_{p \times q}$ such that each column corresponded to an epoch, where p and q denote the number of time points within each epoch and the overall number of slice acquisitions (i.e. all slices for all acquired volumes), respectively. After applying SVD to the data matrix, we further expressed \mathbf{D} as the sum of a set of orthogonal components, $\{\mathbf{C}_i, i = 1, \dots, \min(p, q)\}$, each of which was the product of a unitary column vector \mathbf{u}_i (i.e. the left singular vector) and a unitary row vector \mathbf{v}_i^T (i.e. the right singular vector), scaled by a weighting factor s_i (i.e. the singular value). For each component \mathbf{C}_i , the left singular vector \mathbf{u}_i represented a temporal pattern (or basis function) that spanned the duration of a single slice acquisition, and the right singular vector \mathbf{v}_i reflected the varying amplitude of such a pattern for different acquisitions. Both the left and right singular vectors were orthogonal for different components ($\mathbf{u}_i^T \mathbf{u}_j = 0, \mathbf{v}_i^T \mathbf{v}_j = 0$ for $i \neq j$).

$$\mathbf{D} = \sum_i^{\min(p,q)} \mathbf{C}_i = \sum_i \mathbf{u}_i s_i \mathbf{v}_i^T \quad (1)$$

Following the SVD, we classified one or multiple components as gradient artifacts based on the following rationale and quantitative criterion. Gradient artifacts consisted of temporal patterns that were either relatively stable or slowly variable across slice acquisitions, whereas the temporal patterns of brain signals were independent of the fMRI slice timing and their amplitudes ought to fluctuate around zero across acquisitions. Such distinctions gave important clues to the SVD component classification based on a one-sample t-test applied to the right singular vector \mathbf{v}_i of each component. The t-test used to test whether the mean of the elements in \mathbf{v}_i differed significantly from zero with $p \leq 0.05$ corrected for multiple comparisons. This test evaluated whether the temporal pattern described by the left singular vector \mathbf{u}_i was relatively consistent across slices. A component was classified as artifactual if the t-test attained significance. Fig. 1 illustrates the above procedures with example data recorded during an eyes-closed resting experiment.

From all the artifactual components identified as above, their left singular vectors formed a set of orthogonal basis functions. A linear combination of these functions was expected to fit the gradient artifact induced by the acquisition of any individual slice for the given EEG channel. Therefore, regressing out such a set of basis functions from every epoch of the raw data left behind a continuous time-series of residuals with gradient artifacts being effectively removed or minimized. The data were then low-pass filtered with a cutoff frequency at 125Hz and then down-sampled at 250Hz for the efficiency of data storage and memory usage.

Pulse Artifact Correction

After the gradient artifact removal, we removed the pulse artifact using the following steps: (1) we applied temporal ICA to the data recorded from all EEG channels; (2) we identified the ICs attributable to pulse artifacts based on the normalized mutual information computed between the component time-course and the ECG signal; (3) we identified the R peaks (i.e. the center peak of the QRS complex) based on the ECG signal; (4) we applied a SVD-based filter to the time-course of each IC to remove the reoccurring patterns phase-locked to the R peak; (5) we projected the remaining signals from the component space to the channel space using the inverse transformation of the ICA performed in step (1) after excluding the artifactual ICs identified in step (2). Fig. 2 illustrates these procedures with an example from our recorded data. In what follows, we will describe each of the above steps in detail.

ICA and Component Selection

The time-series data from all the EEG channels (except the ECG and EOG channels) were decomposed into temporally independent components using an extended infomax algorithm implemented in EEGLAB (Delorme and Makeig, 2004). This algorithm minimized the average mutual information shared by every pair of output components (Bell and Sejnowski, 1995). As expressed by Eq. (2), the resulting components comprised a linearly transformed representation of original N -dimensional data, where N was the number of EEG channels.

$$\mathbf{X} = \mathbf{WZ} \quad (2)$$

where \mathbf{Z} is the N -by- T channel-space data matrix (T denotes the number of time points), \mathbf{W} is the linear ICA transformation matrix and \mathbf{X} is the resulting N -by- T component-space matrix.

Since \mathbf{W} is invertible, both forward and inverse transformations exist to relate the channel-space representation to the component-space representation and vice versa. However, the component space is much more effective than the channel space for classifying patterns into distinct classes (i.e. pulse artifacts vs. brain signals). This is because the features represented by individual components are readily disjoint in information, whereas the features represented in the channel space are mixed with large redundancy among channels.

An ensuing problem was how to select the ICs that represented the spatiotemporal features of pulse artifacts as opposed to brain signals. Since pulse artifacts were driven by cardiac activity, we sought a subset of m components (m was unknown) which jointly had the maximal statistical dependency on the ECG. This was equivalent to selecting the m components with the largest mutual information with the ECG, considering that all the output components of ICA were mutually exclusive (Peng et al., 2005). Here both the dependency and redundancy were defined in terms of mutual information, instead of linear cross correlation, in order to reflect the complex and nonlinear relationship between pulse artifacts and ECG. Using an example from our recorded data, Fig. 3 demonstrates the difference in artifactual feature extraction between the channel space and the component space with respect to their mutual information and cross correlation with ECG.

More specifically, given a set of random variables x_i denoting the individual ICs and another random variable y denoting the ECG, the mutual information between x_i and y was defined in terms of their individual probabilistic density functions $p(x_i)$, $p(y)$, and $p(x_i, y)$.

$$I(x_i; y) = \iint p(x_i, y) \log \left[\frac{p(x_i, y)}{p(x_i)p(y)} \right] dx_i dy \quad (3)$$

Note that $\log[\cdot]$ in Eqs. (3) and (4) computes the natural logarithm. The mutual information $I(x_i; y)$ measured the reduced uncertainty in the time-course of each component due to the known ECG. We further normalized $I(x_i; y)$ by the entropy of x_i (i.e. the total uncertainty associated with x_i) to allow for the comparison across components.

$$J(x_i; y) = -I(x_i; y) / \int p(x_i) \log[p(x_i)] dx_i \quad (4)$$

Note that the probability density and integral operation in Eq. (3) and Eq. (4) were time-consuming to compute since the variables x_i and y were continuous. In practice, the values of each variable were grouped into discrete bins, each of which had a range of 1/5 the standard deviation of the variable. This discretization served to approximate the continuous signals by discrete counterparts such that the probability density function and the integral operation could be simplified as histogram and summation, respectively.

To select the m artifactual components with maximal joint dependency with the ECG, we sought the top m components in the descent ordering of $J(x_i; y)$. However, m was unknown *a priori*. To resolve this issue we used an incremental selection scheme modified from the feature selection method proposed in (Peng et al., 2005). This method aimed to determine the number of artifactual components, m , that resulted in the smallest error in leave-one-out cross-validation. For this cross-validation purpose, we divided the time series of all the

components into 20-s segments with 10-s overlap. Starting from $m = 1$, we randomly selected a single segment as the testing data and use the remaining segments as the training data. For both training and testing data the mutual information with the ECG was computed. The m components with the highest mutual information in training and testing data were then compared to see if they were identical. We repeated this procedure for every segment to serve once as the testing data. Finally, we computed the overall cross-validation error as the percentage of cases in which the component groups derived for the training and testing sets were inconsistent. Subsequently, m was incrementally increased until the cross validation error was greater than 50%. This gave rise to n sequentially expanding component sets $S_1 \subset S_2 \subset \dots \subset S_m$, from which we sought the best set S_m ($m \leq n$) that gave the smallest error in cross validation. If the smallest error was greater than 10%, no component was excluded as artifactual. If more than one component set had the equally smallest classification error, we chose the one that contained relatively more components. This incremental selection scheme ensured the identification of a compact cluster of components that was strongly and constantly dependent on the ECG with high mutual information clearly distinctive from those of other components. In other words, the difference in mutual information was relatively smaller within the selected artifact component set than between the artifact and non-artifact sets.

R-peak detection

We identified a time marker for every heart beat by detecting the R peaks in the ECG trace recorded inside the scanner. In order to facilitate the R-peak detection, we first amplified the R-wave while suppressing other ECG components, especially the T-wave, whose amplitude was greatly elevated by the magnetic field (Laudon et al., 1998). Specifically, we band-pass filtered the ECG signal from 8 to 40 Hz, and then applied the Teager energy operator (TEO) (Kim et al., 2004; Maragos et al., 1993; Niazy et al., 2005) to the filtered ECG. The above cutoff frequencies were chosen to separate the R wave from other ECG components since the former had a relatively shorter duration and higher frequency. The TEO operator served to further amplify all the spikes relative to the baseline signal. Fig. 4 illustrates the effects of the band-pass filtering and TEO with an example from our recorded data.

Let $y(t)$ denote the input signal (e.g. the filtered ECG signal), the TEO operator $\psi(\cdot)$ is expressed as Eq. (5). The output signal is roughly proportional to the instantaneous power and frequency content of the input signal (Maragos et al., 1993; Mukhopadhyay and Ray, 1998).

$$\psi[y(t)] = y^2(t) - y(t-1)y(t+1) \quad (5)$$

After the above filtering and transformation, identifying the R peaks in the resulting TEO signal was equivalent to, yet much easier than, identifying the R peaks in the original ECG signal. To do so, we developed an algorithm combining both amplitude-based peak detection and correlation-based template matching. We first estimated the R-R interval (RRI) based on the autocorrelation function of the TEO signal. Assuming that the heart rate ranged from 40 to 120 beats per minute, the RRI should accordingly range from 0.5 to 1.5 s. Within this initial range, the average RRI was estimated to be the positive time lag with the maximal autocorrelation coefficient. To further estimate the R-peak height, we evenly divided the TEO signal into non-overlapping segments, each of which was $2 \times \text{RRI}$ long so as to contain at least one R-peak. We collected a set of samples for the R-peak height by taking the maximum amplitude from every segment, and then excluded the outliers from this sample set by removing the elements either greater than the third quartile or less than the first quartile by three times the inter-quartile range. The minimum and maximum of the

remaining samples provided an expected range for the amplitude of any R-peak. We then identified all the positive peaks within this amplitude range as the candidates for the R peaks.

In addition, we used correlation-based template matching to further confirm or reject the R-peak candidates found with the above amplitude-based peak detection, which likely led to misidentification of some spurious spikes due to high-frequency noise interference (e.g. from residual gradient artifacts). A template was automatically chosen from the TEO signal during a single cardiac cycle: the template was centered at the time point with the maximal amplitude (presumably an R peak) during the first 5s TEO signal while the template length was set equal to the average RRI. We derived a time-series of correlation coefficients computed between the template and the signal within a sliding window of the same length, running from the beginning to the end of the TEO signal by one time point per step. We detected all the positive peaks on the cross-correlation time-series above a threshold of 0.7. An R-peak marker was placed if both the amplitude and correlation-based criteria were satisfied.

SVD-based filter

Similar to the gradient artifact removal, we used a SVD-based filter to remove from the component time series those temporal patterns that were phase-locked to the R peaks. Briefly, we segmented the time-course of each component into epochs according to the R-peak positions. Each epoch had a fixed length equal to the average RRI and was centered around each R-peak plus a time delay. This time delay was made to account for the time for blood flow to travel from the heart to the head, and it was determined by maximizing the average signal energy at the epoch center. We performed SVD to the matrix composed by all the segmented epochs, and identified the SVD components that characterized the reoccurring pulse artifact by using the same statistic test as that used in the gradient artifact removal. The left singular vectors of the artifactual SVD components were then regressed out from the component time-series. Such a SVD-based filtering was repeated for every component obtained by the ICA.

PA-Component Removal

After the component time-course was filtered using the SVD-based filter, we transformed the data from the component space back to the original channel space after excluding those PA-related components selected based on their mutual information with the ECG. This inverse transformation was achieved through a linear matrix $\mathbf{R} = \mathbf{W}^{-1}$. The corrected EEG signals (denoted as \mathbf{Z}') were obtained using the following equation.

$$\mathbf{Z}' = \sum_{i \in S_m} \mathbf{r}_i \mathbf{x}'_i \quad (6)$$

where \mathbf{x}'_i is a 1-by- T row vector denoting the time-course of the i -th component after the SVD-based filtering, \mathbf{r}_i is an N -by-1 column vector denoting the i -th column of \mathbf{R} and S_m is the PA-related component set.

Both the PA-related IC removal and the SVD-based filter were needed for a complete removal of pulse artifacts. The SVD filter was effective for removing the temporal patterns that remained stable or slowly variable across heart beats, whereas the irregularity of pulse artifacts and the ECG itself likely led to residual artifacts that were not phase-locked to the R peaks. In contrast, the artifactual components obtained by ICA had constantly high mutual information with the ECG. The cross validation criterion used in the component selection

ensured that the selected artifactual components were independent of the time period based on which the mutual information was calculated. In other words, the artifactual components possessed a stable temporal dependency with the ECG, despite the fact that both the ECG and the component time course could be highly irregular. Therefore, the PA-related IC removal and the SVD-based filter were used to remove the irregular and regular patterns of pulse artifacts, respectively.

Comparison with alternative methods

We also used two other commonly used methods to remove gradient and pulse artifacts. The first method was based on AAS (Allen et al., 2000) implemented in BrainVision Analyzer (version 1.05, BrainVision LLC); the second method was based on the so-called optimal basis sets (OBS) (Niazy et al., 2005) implemented in an EEGLAB plug-in toolbox (FMRIB, Oxford University). We compared these two methods with the method proposed in this paper. All three methods were applied using the default settings as described in the original two papers (Allen et al., 2000; Niazy et al., 2005) and the settings mentioned in this manuscript for the method described here. The strategy for the method comparison is described below.

We measured the level of pulse artifact reduction by using the Improvement in terms of Normalized Power Spectrum (INPS), which is the normalized power spectrum ratio before and after applying correction, as was previously proposed in (Tong et al., 2001). This method was also adopted in several other studies dealing with simultaneous EEG-fMRI recordings (Briselli et al., 2006; Leclercq et al., 2009; Nakamura et al., 2006; Rasheed et al., 2009; Srivastava et al., 2005). Specifically, we summed the spectral powers at the multiples of heart rate (up to the 5th harmonic) for the EEG before and after pulse artifact correction and then computed the ratio between them. A higher INPS indicates a greater degree of pulse artifact reduction. The INPS was computed separately for each method under comparison.

For one subject (arbitrarily selected from our subject pool) from which the same visual stimulation paradigm was repeated inside and outside of the scanner, we computed the residual errors as the difference between the VEP signals recorded inside and outside of the scanner. The variance of the residual errors was computed for every channel and the mean variance averaged across channels was calculated for each method under comparison.

In addition to the above experiment or analysis specifically for the method comparison, we also selected a few representative examples of the data processed with different artifact correction algorithms for a qualitative comparison of these methods on a case by case basis.

RESULTS

Fig. 5 demonstrates the efficacy of the proposed gradient artifact and pulse artifact removal with example time-series data acquired from a single subject performing a behavior task with alternating eyes-closed and eyes-open periods. The raw data contained reoccurring artifactual patterns with amplitudes significantly greater than the true EEG signals (Fig. 5.a). The SVD-based filter removed the gradient artifacts nearly entirely, resulting in much clearer signals yet still contaminated by pulse artifacts with amplitudes and shapes varying across channels (Fig. 5.b). After the pulse artifact was also removed, the corrected EEG traces showed alpha oscillations predominantly at occipital and parietal channels (Fig. 5.c). Such alpha oscillations sustained during the eyes-closed period and were suppressed during the eyes-open period with a clear transition observable around 5.6s when the subject opened the eyes.

Fig. 6 shows the power spectral density function of the time-series data partly displayed in Fig. 5. The gradient artifacts manifested themselves as spectral peaks at multiples of the slice repetition frequency (i.e. the number of slices per volume divided by TR) (Fig. 6.a). When the fMRI scans were continuous in time, these spectral peaks had very narrow bandwidths and minimal interference with brain signals at other frequencies. As a time-domain filter, the SVD-based filter effectively eliminated the spectral peaks at the primary slice repetition frequency (dashed lines) and its harmonics (not shown) without any noticeable effect on other spectral components (Fig. 6.b). However, the power spectra after gradient artifact removal appeared highly similar with that of the ECG (Fig. 6.d), suggesting the presence of strong artifacts related to cardiac pulsation. The spectral signature of pulse artifacts included multiple spectral components at the cardiac frequency (dotted lines) and its harmonics. These components have relatively broader bandwidths and largely interfered with and obscured the major frequency components of brain signals. The proposed pulse artifact removal algorithm unveiled the true EEG spectra (Fig. 6.c), clearly revealing two spectral components peaked at the low alpha band (8–10Hz) and high alpha band (10–13Hz).

Fig. 7 displays the spectrogram representing the power as a function of time and frequency at the middle occipital channel Oz for the data acquired (on a different subject) during an eyes-closed-eyes-open task (Fig. 7.a). Such a task was expected to generate a spectral contrast in the alpha-band power between the eyes-closed and eyes-open periods (i.e. higher alpha power when eyes were closed vs. lower alpha power when eyes were open). The expected alpha alteration was not seen in the spectrogram with the presence of pulse artifacts (Fig. 7.b). After the pulse artifacts were corrected by applying the SVD filter to the time-series data represented in the original channel space (Fig. 7.c) or in the ICA-transformed component space (Fig. 7.d), the expected alpha contrast became visible but noisy. The SVD filtering in the component space was slightly superior to the same filtering applied to the channel space. In this example, simply removing the artifactual ICs identified according to their mutual information with the ECG provided improved alpha contrast (Fig. 7.e), whereas residual pulse artifacts were still observable at multiple harmonics of the cardiac frequency. In contrast, these residuals were not seen in the corrected spectrogram after we both applied the SVD filter to the component time series and removed the PA-related components (Fig. 7.f). Such a combined method for pulse artifact correction led to the highest spectral contrast in the alpha band as well as its second harmonic.

We also tested the proposed algorithm with an event-related paradigm. Fig. 8 shows the visual evoked potential (VEP) induced by 2Hz full-field visual stimuli for a (different) single subject. The VEP response was strongest at occipital electrodes (Fig. 8.a) with three components following the stimulus onset: a negative peak at 83ms, a positive peak at 107ms and another negative peak at 142ms (Fig. 8.b). These components were respectively consistent with the N75, P100 and N145 components of pattern-reversal VEP in terms of both polarity and latency (Di Russo et al., 2005). Moreover, these three components were observable not only in the average VEP response but also in the single-trial responses (Fig. 8.b), suggesting a high SNR attained by the proposed algorithm.

We further evaluated the spectral specificity achieved by the proposed methods by using a visual paradigm designed to induce steady state visual evoked potentials (SSVEP). Since visual stimulation at a fixed temporal frequency is known to evoke occipital electrical responses with the same frequency, we used such stimulation to generate spatially and spectrally specific contrast against the stimulus-free control condition. Fig. 9 shows the spectral topographies and time courses of the SSVEP obtained from two subjects presented with visual stimulation at 6 or 10Hz (Fig. 9.a and Fig. 9.b respectively). The spectral difference between the periods with and without visual stimulation showed sharp peaks at

the stimulus frequency for the three occipital channels (O1, Oz and O2). From these channels, the electrical potentials averaged with respect to the stimulus onset showed reoccurring responses evoked by repetitive visual stimuli. Consistent results were found for both 6 and 10Hz stimuli.

For the above example data sets, we also applied two other published methods (AAS and OBS) for artifact correction and compared the results with those obtained with our proposed method. For the alpha power response induced by the eyes-open-eyes-closed task, the time-frequency spectrograms obtained with AAS and OBS are shown in Fig. 7.g) and 7.h), respectively. The alpha-band spectral contrast between the eyes-closed and eyes-open periods (computed with two-sample t-test) was lower for AAS ($t=13.19$) and OBS ($t=11.47$) than for the proposed method ($t=16.45$). For the 2-Hz visual stimulation experiment, the VEP responses obtained with AAS and OBS are shown in Fig. 8.c) and 8.d), respectively. We quantified the signal-to-noise ratio for N75, P100 and N145 components in the average VEP responses. This was done by dividing the absolute peak amplitude of each component by the noise level estimated from the standard deviation of the signal amplitudes from -100 ms to 50 ms relative to stimulus onset. The estimated noise level was 0.40 for the proposed method, 0.86 for AAS and 1.00 for OBS. The average component SNR was 8.90 for the proposed method, 5.66 for AAS and 3.64 for OBS. In addition, it is readily observable that the proposed method gave rise to less variation in single-trial VEP responses to individual stimuli relative to AAS and OBS. Quantitatively, the average trial-to-trial variation was 0.35 for the proposed method, 0.96 for AAS and 0.93 for OBS. For the visual evoked response to 6 Hz visual stimulation (Fig. 10), the proposed method gave rise to a steady SSVEP time course, whereas the SSVEP time courses for AAS and OBS seemed more variable. The SSVEP spectra obtained with the proposed method and OBS were comparable, while AAS was less satisfactory. In short, for these cases the proposed method performed better than or equivalent to the two alternative methods in terms of preserving the spatial, temporal and spectral features of EEG and event-related potentials (ERP).

For a different single subject, we also compared the resting EEG spectrum and time series among three recording conditions: 1) with fMRI, 2) inside the scanner without fMRI, 3) outside the scanner. As shown in Fig. 11.a), all three methods performed reasonably well in the removal of gradient artifacts, except that the OBS method seemed to overcorrect the gradient artifact by removing additional EEG signals at multiples of a half of the slice repetition frequency. For the PA removal in this example, the difference between these three methods was obvious (Fig. 11.b). Temporally, our proposed method removed more signals than the other two methods while preserving the alpha oscillation that was expected to dominate the posterior EEG at rest. Spectrally, a peak around 10.5 Hz was clearly visible in the data obtained with our proposed method. This spectrum was similar to the EEG spectrum obtained outside the MRI scanner but with smaller alpha peak amplitude. While the AAS and OBS methods also preserved the alpha components, their resulting spectra showed spurious low-frequency (3 – 8 Hz) components that were absent in the clean EEG spectrum.

For another different subject, we compared the task-induced alpha modulation and VEP signals recorded inside and outside the MRI scanner. As shown in Fig. 12, the proposed method revealed a clear alpha-power modulation as a result of opening and closing the eyes. Such a modulation recorded inside the scanner appeared very strong and specific to the alpha band, similar to that recorded outside the scanner. Note that as the task was self-paced by the subject, the subject opened and closed the eyes at different times for the experiments performed inside and outside the MR scanner. However, the alpha modulation obtained with AAS or OBS was either less specific to the alpha band or much weaker, respectively. The

quantified alpha contrast obtained with the proposed method and AAS were comparable to that recorded outside the scanner, whereas OBS resulted in a much lower alpha contrast.

The comparison between the VEP recorded inside the scanner with different artifact correction methods and the VEP recorded outside the scanner is shown in Fig. 13. From the VEP channel plots (Fig. 13.A through D), we can see that the VEP obtained with the proposed method and using AAS were comparable to the VEP recorded outside the scanner, whereas OBS was much less satisfactory. This can be confirmed by the VEP comparison at a single channel Pz (Fig. 13.E). We calculated the residual errors as the difference between the VEP recorded inside and outside the scanner. For each channel, the residual error was quantified by its variance. The mean variance of residual errors was further computed by averaging the variance across all channels. The quantified residual error was lower for the proposed method relative to the two alternative methods.

For each of the three methods under comparison (i.e. the proposed method, AAS and OBS), we computed INPS for all of our datasets ($n=204$ combined for all subjects), regardless of the experimental paradigm used. The proposed method resulted in the highest INPS for 79.4% of the datasets, in contrast to 3.6% for AAS and 17% for OBS. Overall the proposed method (INPS= 29.2 ± 2.1) gave rise to a significantly greater degree of pulse artifact suppression than both AAS (INPS= 11.1 ± 0.7) and OBS (13.3 ± 0.8).

DISCUSSION

We presented a method for improved artifact removal from EEG data collected within the MRI scanner. The sample results of this method presented above demonstrate the effectiveness of the method in removing artifacts resulting from MRI gradient switching and cardiac pulsation. We have applied these algorithms to about 200 sessions of simultaneous EEG-fMRI recordings collected from a group of healthy human subjects using a 32-channel EEG system within a 3T MRI scanner across a variety of experimental paradigms. High quality data were reliably obtained for all of these sessions. Our implementation of the proposed algorithm is fully automatic and has no requirement for user-specific parameter setting. Below specific aspects of our method are contrasted with those in previously published methods, and potential directions of future development are suggested.

Gradient Artifact Removal

Perhaps the most widely used method for gradient artifact removal is the average artifact subtraction (AAS) method (Allen et al., 2000). In AAS, a local artifact template is computed for each EEG channel as the signal average with respect to the onset times of the fMRI slices acquired within a sliding time window. Depending on an empirical choice, the length of the sliding window is critical in balancing brain signal loss and gradient artifact variability. On one hand, it is desirable to use a long sliding window to cover a sufficient number of slice acquisitions so that brain signals can be averaged out of the computed template and thus not removed; on the other hand, a short sliding window is desirable to obtain a more local artifact template that is better suited to filter out a variable gradient artifact but risks some loss of brain signals. The examples shown in Fig. 14 demonstrate the effect of the window length on the spectrum of EEG after the AAS-based GA removal: a short moving window resulted in over-correction whereas a long window resulted in under-correction. Therefore the choice of window length is a compromise between optimally removing stationary and variable gradient artifacts. This limitation often leads to unsatisfactory artifact removal by using AAS or its variations (Goldman et al., 2000; Goncalves et al., 2007; Sijbers et al., 1999).

The proposed SVD-based filter overcomes this limitation. The SVD filter uses data for all slice acquisitions to maximize the statistical power desired in order to avoid the removal of brain signals, whereas more than one SVD component can be selected to account for the temporal variability of gradient artifacts. Similar ideas have been adopted by other groups for the removal of gradient artifacts (Mandelkow et al., 2010; Negishi et al., 2004; Niazy et al., 2005). However, two distinctions from these methods should be noted. In previous methods, SVD (or equivalently PCA) is applied to the channel-wise signals that remain after AAS. Although these methods may help reduce the residual artifacts uncorrected by AAS, there is obviously no way to undo the possible removal of brain signals resulting from AAS. Second, quantitative criteria for artifactual component selection are either lacking or loosely defined (Mandelkow et al., 2010; Negishi et al., 2004; Niazy et al., 2005). For example, Niazy et al. propose to remove the first SVD component (or the first few) that explains the highest variance of the residual signal after AAS. This likely leads to over-correction (see Fig. 11.a for an example) because the first few SVD components always explain more variance than other components regardless of whether there are uncorrected artifacts in the signal or not.

In some previous studies, signal processing solutions are developed to deal with the difficulty of gradient artifact removal resulting from the misalignment of EEG and MRI data samples due to slightly differing sampling frequencies (Mandelkow et al., 2010; Niazy et al., 2005; Ryali et al., 2009; Wan et al., 2006). These solutions are commonly based on slightly shifting the MRI trigger positions to improve the phase-locking of gradient artifacts with respect to the triggers. In our study, we did not do such processing; instead a device was used to physically synchronize EEG and MRI sampling clocks. Since such a hardware solution is increasingly available, it eliminates the source of non-synchronization and thus is obviously more desirable than any retrospective correction. Nevertheless, the proposed SVD filter is capable of removing gradient artifacts even with imperfect synchronization.

In the present study, the gradient artifact is removed channel by channel. This ignores the strong dependency of the artifacts experienced by different channels. We anticipate that such spatial dependency would be helpful to further improve the artifact removal. Recall again that the artifactual voltage is proportional to the changing rate of the magnetic flux, which depends on the area enclosed by the conductive loops and the magnetic field inside it. As the change of the looped area is much slower than the change of magnetic field gradients, the gradient artifact depends almost entirely on the changing rate of magnetic field gradients. Note that there are only three gradients in place along three orthogonal directions. The gradient artifacts induced by any single slice acquisition at tens of electrodes should reflect at most three template patterns, each of which corresponds to one gradient direction. Although we did not utilize this spatial dependency in our study because the proposed SVD filter seems sufficient for retrospective removal of gradient artifacts, it may be very helpful for real-time removal of gradient artifacts. We would like to explore this in future studies.

Pulse Artifact Correction

To facilitate pulse artifact correction, TEO is helpful for detecting the R peaks. In two previous papers (Kim et al., 2004; Niazy et al., 2005), a modified TEO (called k -TEO) is suggested to outperform TEO based on the argument that an appropriately selected k enables the frequency selectivity desirable for the R-peak amplification. We argue here that such a modification is unnecessary if the ECG signal is first band-pass filtered from 8 to 40 Hz, whereas an improperly selected k value would likely confound the R peak detection by amplifying the high-frequency noise. In addition, we chose not to use the algorithm reported in (Christov, 2004; Niazy et al., 2005), which allows for real-time QRS detection but requires the setting of many parameters and is computationally demanding given a long

recording period. In contrast, our proposed R-peak detection takes only several seconds on average on a typical Linux workstation.

We used ICA for the extraction of the features characterizing pulse artifacts or brain signals. Although ICA has been used in the correction of pulse artifacts (Benar et al., 2003; Debener et al., 2007; Leclercq et al., 2009; Mantini et al., 2007; Nakamura et al., 2006; Srivastava et al., 2005; Vanderperren et al., 2010), previous studies face the uncertainty as to which components are artifactual and thereby need to be removed. This uncertainty puts ICA at risk for undesired removal of brain signals (Vanderperren et al., 2010). To overcome this problem, we introduced mutual information based criteria to select a compact cluster of components with maximal joint dependency on ECG while such dependency remained high over time. Our results demonstrate that mutual information is preferable to cross correlation for measuring the complex relationship between pulse artifacts and ECG. However, component selection based on mutual information is very conservative and cannot completely account for all pulse artifacts. This is partly due to the large spatial variation in the amplitude, arrival time and shape of the pulse artifacts experienced at different channels. As a result, other components that are not selected for removal also contain some portions of pulse artifacts, albeit to relatively lesser extent. These remaining artifacts are removed by applying the proposed SVD filter to the time course of every component. Complementary to ICA, the SVD filter makes it less critical for the uncertain classification of some components, which are partly artifacts and partly brain signals, as components of brain signals instead of pulse artifacts. In short, ICA removes the patterns that change over time, and SVD removes remaining coherent patterns.

Note that we applied the SVD filter to the time-series data represented in the component space, in contrast to some previous studies in which the SVD filtering is performed in a channel-wise basis (Debener et al., 2008; Niazy et al., 2005). We prefer to apply the SVD filter to the component space rather than the channel space mainly for two reasons. First, the ICA redistributes pulse artifacts in the component space so some components end up with more artifacts than others. This is in contrast to the channel space in which pulse artifacts are relatively evenly distributed across channels. Therefore, the application of ICA before the SVD filtering provides differing artifact-to-signal ratio for individual components. For the components that contain more pulse artifacts than others, its higher artifact-to-signal ratio results in the higher statistical power that is needed to confidently separate more artifacts from signals in the SVD. Second, ICA generates mutually independent time courses. In every component time course, the SVD components determined as artifactual are independent as well. Regressing out these artifactual SVD components from an individual ICA component leads to regressing them out from all channel-wise time courses, as the inverse ICA is a linear transformation. After this SVD filtering is applied to all the ICA components, one has effectively filtered the time course of every channel with a large group of independent basis functions, which collectively give a better fit to the temporally variable pulse artifact than the basis functions that are directly derived from the channel-wise time course.

Quantitative Comparison with Alternative Methods

In the present study, the evaluation of the proposed method in contrast to other alternative methods remains mostly qualitative. Considering this limitation we tend to be cautious and avoid concluding that the proposed method performs significantly better than other existing methods. A more comprehensive and quantitative evaluation is certainly desirable yet very difficult to perform. The difficulty is largely due to the lack of absolute gold standard, or 'truth' measurement, to which the data processed with different methods can be quantitatively compared to and thus assessed. A few comparative studies have focused on quantifying and comparing the performance of a couple of existing methods for removing

gradient artifacts. For example, Ritter and colleagues used an interleaved fMRI acquisition and compared the EEG signal spectra during the alternating periods with and without gradient switching (Ritter et al., 2007). We did not use the interleaved acquisition because it would introduce some dispersion of the artifact spectrum (Mandelkow et al., 2010) and limit our ability in investigating the low-frequency signals. Moreover, the gradient artifact removal is less of concern especially when hardware for the MRI-EEG clock synchronization is in use. In our opinion the hardware solution is more preferable than any retrospective signal processing solution for dealing with the clock asynchrony, which would otherwise be avoided.

The performance quantification for pulse artifact correction is more important and obviously more challenging. One may argue that EEG signals recorded outside the MRI scanner would serve as the reference signals to which EEG signals recorded inside the scanner can be quantitatively compared. One such experiment was included in this work and some other groups have also done such comparisons. For example, Im and colleagues have quantitatively compared the visual evoked potentials recorded inside and outside of the MRI scanner, as well as the cortical activity reconstructed from these signals (Im et al., 2006). While major temporal and spatial features were overall similar, discrepancies in details (e.g. absolute signal amplitude and duration, spatial extent and location) were obvious. Some may quantify such discrepancies to measure the error of the artifact correction algorithm used. However, we always need to keep in mind the confounding difference in the experimental condition (e.g. stimulus setting and subject position) and the subject's mental state (e.g. attention and vigilance) may also account for the difference between the signals inside and outside of the scanner. In addition, other quantitative measures (e.g. INPS used in this study) can only measure one aspect of artifact correction and are as such not completely indicative of the performance of correction methods in general.

Another practical issue is concerned with the fairness of comparison between individual algorithms. A fair comparison cannot be reached until individual methods are optimized, which would be ideally done by their developers. A fair comparison would need a variety of data sets so as to avoid the use of selected data that are favorable for some algorithms yet against the others. A fair comparison would also need the efforts to make individual algorithms publically accessible in order for other independent users to test for reproducibility. A multi-laboratory collaborative effort would ideally be the basis of such a quantitative comparison, putting this outside of the scope of the current work. It is perhaps all of the aforementioned concerns that amount to a still unresolved question as to which algorithm should be used for simultaneous EEG-fMRI studies, despite the previous efforts along this direction.

CONCLUSION

A set of refined algorithms has been developed to remove gradient and pulse artifacts from EEG recordings simultaneously acquired with continuous fMRI scans. The developed algorithms rest on advanced statistical methods for the automatic extraction and selection of artifactual features, and have been demonstrated to provide excellent quality for data collected with a variety of paradigms including resting-state, behavioral tasks, sensory stimulation, etc. The algorithms described herein have also been implemented in a Matlab-based toolbox available for public access and research use. We believe that this toolbox will further advance our existing ability in multimodal neuroimaging combining EEG and fMRI, which are often desirable in both neuroscience and clinical applications.

Acknowledgments

The authors appreciate Dr. Hanchuan Peng for kindly sharing his C program for computing entropy and mutual information, Dr. Masaki Fukunaga and Susan Guttman for their assistance in data collection and Drs. Qi Duan and Hendrik Mandelkow for useful discussions and carefully reading this manuscript. This research was supported by the Intramural Research Program of the National Institute of Neurological Disorders and Stroke, National Institutes of Health.

References

- Allen PJ, Josephs O, Turner R. A method for removing imaging artifact from continuous EEG recorded during functional MRI. *Neuroimage*. 2000; 12:230–239. [PubMed: 10913328]
- Allen PJ, Polizzi G, Krakow K, Fish DR, Lemieux L. Identification of EEG events in the MR scanner: the problem of pulse artifact and a method for its subtraction. *Neuroimage*. 1998; 8:229–239. [PubMed: 9758737]
- Anami K, Mori T, Tanaka F, Kawagoe Y, Okamoto J, Yarita M, Ohnishi T, Yumoto M, Matsuda H, Saitoh O. Stepping stone sampling for retrieving artifact-free electroencephalogram during functional magnetic resonance imaging. *Neuroimage*. 2003; 19:281–295. [PubMed: 12814579]
- Bell AJ, Sejnowski TJ. An information-maximization approach to blind separation and blind deconvolution. *Neural Comput*. 1995; 7:1129–1159. [PubMed: 7584893]
- Benar CG, Aghakhani Y, Wang YH, Izenberg A, Al-Asmi A, Dubeau F, Gotman J. Quality of EEG in simultaneous EEG-fMRI for epilepsy. *Clinical Neurophysiology*. 2003; 114:569–580. [PubMed: 12705438]
- Briselli E, Garreffa G, Bianchi L, Bianciardi M, Macaluso E, Abbafati M, Marciante MG, Maraviglia B. An independent component ballistocardiogram analysis-based approach on artifact removing. *Magnetic Resonance Imaging*. 2006; 24:393–400. [PubMed: 16677945]
- Christov II. Real time electrocardiogram QRS detection using combined adaptive threshold. *Biomed Eng Online*. 2004; 3:28. [PubMed: 15333132]
- Debener S, Mullinger KJ, Mazy RK, Bowtell RW. Properties of the ballistocardiogram artefact as revealed by EEG recordings at 1.5, 3 and 7 T static magnetic field strength. *International Journal of Psychophysiology*. 2008; 67:189–199. [PubMed: 17683819]
- Debener S, Strobel A, Sorger B, Peters J, Kranczioch C, Engel AK, Goebel R. Improved quality of auditory event-related potentials recorded simultaneously with 3-T fMRI: Removal of the ballistocardiogram artefact. *Neuroimage*. 2007; 34:587–597. [PubMed: 17112746]
- Delorme A, Makeig S. EEGLAB: an open source toolbox for analysis of single-trial EEG dynamics including independent component analysis. *J Neurosci Methods*. 2004; 134:9–21. [PubMed: 15102499]
- Di Russo F, Pitzalis S, Spitoni G, Aprile T, Patria F, Spinelli D, Hillyard SA. Identification of the neural sources of the pattern-reversal VEP. *Neuroimage*. 2005; 24:874–886. [PubMed: 15652322]
- Ellingson ML, Liebenthal E, Spanaki MV, Prieto TE, Binder JR, Ropella KM. Ballistocardiogram artifact reduction in the simultaneous acquisition of auditory ERPS and fMRI. *Neuroimage*. 2004; 22:1534–1542. [PubMed: 15275910]
- Freyer F, Becker R, Anami K, Curio G, Villringer A, Ritter P. Ultrahigh-frequency EEG during fMRI: pushing the limits of imaging-artifact correction. *Neuroimage*. 2009; 48:94–108. [PubMed: 19539035]
- Goldman RI, Stern JM, Engel J, Cohen MS. Acquiring simultaneous EEG and functional MRI. *Clinical Neurophysiology*. 2000; 111:1974–1980. [PubMed: 11068232]
- Goncalves SI, Pouwels PJW, Kuijter JPA, Heethaar RM, de Munck JC. Artifact removal in co-registered EEG/fMRI by selective average subtraction. *Clinical Neurophysiology*. 2007; 118:2437–2450. [PubMed: 17889599]
- Grouiller F, Vercueil L, Krainik A, Segebarth C, Kahane P, David O. A comparative study of different artefact removal algorithms for EEG signals acquired during functional MRI. *Neuroimage*. 2007; 38:124–137. [PubMed: 17766149]
- He B, Liu Z. Multimodal Functional Neuroimaging: Integrating Functional MRI and EEG/MEG. *IEEE Rev Biomed Eng*. 2008; 1:23–40. [PubMed: 20634915]

- Huang-Hellinger FR, Breiter HC, McCormack G, Cohen MS, Kwong KK, Sutton JP, Savoy RL, Weisskoff RM, Davis TL, Baker JR, Belliveau JW, Rosen BR. Simultaneous functional magnetic resonance imaging and electrophysiological recording. *Human Brain Mapping*. 1995; 3:13–23.
- Im CH, Liu Z, Zhang N, Chen W, He B. Functional cortical source imaging from simultaneously recorded ERP and fMRI. *J Neurosci Methods*. 2006; 157:118–123. [PubMed: 16675026]
- Jain AK, Duin RPW, Mao JC. Statistical pattern recognition: A review. *Ieee Transactions on Pattern Analysis and Machine Intelligence*. 2000; 22:4–37.
- Kim KH, Yoon HW, Park HW. Improved ballistocardiac artifact removal from the electroencephalogram recorded in fMRI. *Journal of Neuroscience Methods*. 2004; 135:193–203. [PubMed: 15020103]
- Laudon MK, Webster JG, Frayne R, Grist TM. Minimizing interference from magnetic resonance imagers during electrocardiography. *IEEE Trans Biomed Eng*. 1998; 45:160–164. [PubMed: 9473839]
- Laufs H, Daunizeau J, Carmichael DW, Kleinschmidt A. Recent advances in recording electrophysiological data simultaneously with magnetic resonance imaging. *Neuroimage*. 2008; 40:515–528. [PubMed: 18201910]
- Leclercq Y, Balteau E, Dang-Vu T, Schabus M, Luxen A, Maquet P, Phillips C. Rejection of pulse related artefact (PRA) from continuous electroencephalographic (EEG) time series recorded during functional magnetic resonance imaging (fMRI) using constraint independent component analysis (cICA). *Neuroimage*. 2009; 44:679–691. [PubMed: 19015033]
- Mandelkow H, Brandeis D, Boesiger P. Good practices in EEG-MRI: the utility of retrospective synchronization and PCA for the removal of MRI gradient artefacts. *Neuroimage*. 2010; 49:2287–2303. [PubMed: 19892021]
- Mandelkow H, Halder P, Boesiger P, Brandeis D. Synchronization facilitates removal of MRI artefacts from concurrent EEG recordings and increases usable bandwidth. *Neuroimage*. 2006; 32:1120–1126. [PubMed: 16861010]
- Mantini D, Perrucci MG, Cugini S, Ferretti A, Romani GL, Del Gratta C. Complete artifact removal for EEG recorded during continuous fMRI using independent component analysis. *Neuroimage*. 2007; 34:598–607. [PubMed: 17112747]
- Maragos P, Kaiser JF, Quatieri TF. On Amplitude and Frequency Demodulation Using Energy Operators. *Ieee Transactions on Signal Processing*. 1993; 41:1532–1550.
- Moosmann M, Schonfelder VH, Specht K, Scheeringa R, Nordby H, Hugdahl K. Realignment parameter-informed artefact correction for simultaneous EEG-fMRI recordings. *Neuroimage*. 2009; 45:1144–1150. [PubMed: 19349230]
- Mukhopadhyay S, Ray GC. A new interpretation of nonlinear energy operator and its efficacy in spike detection. *IEEE Trans Biomed Eng*. 1998; 45:180–187. [PubMed: 9473841]
- Nakamura W, Anami K, Mori T, Saitoh O, Cichocki A, Amari S. Removal of ballistocardigram artifacts from simultaneously recorded EEG and fMRI data using independent component analysis. *Ieee Transactions on Biomedical Engineering*. 2006; 53:1294–1308. [PubMed: 16830934]
- Negishi M, Abildgaard M, Nixon T, Constable RT. Removal of time-varying gradient artifacts from EEG data acquired during continuous fMRI. *Clinical Neurophysiology*. 2004; 115:2181–2192. [PubMed: 15294222]
- Niazy RK, Beckmann CF, Iannetti GD, Brady JM, Smith SM. Removal of FMRI environment artifacts from EEG data using optimal basis sets. *Neuroimage*. 2005; 28:720–737. [PubMed: 16150610]
- Peng H, Long F, Ding C. Feature selection based on mutual information: criteria of max-dependency, max-relevance, and min-redundancy. *IEEE Trans Pattern Anal Mach Intell*. 2005; 27:1226–1238. [PubMed: 16119262]
- Rasheed T, Lee YK, Lee SY, Kim TS. Attenuation of artifacts in EEG signals measured inside an MRI scanner using constrained independent component analysis. *Physiological Measurement*. 2009; 30:387–404. [PubMed: 19321919]
- Ritter P, Becker R, Graefe C, Villringer A. Evaluating gradient artifact correction of EEG data acquired simultaneously with fMRI. *Magnetic Resonance Imaging*. 2007; 25:923–932. [PubMed: 17462844]

- Ritter P, Villringer A. Simultaneous EEG-fMRI. *Neuroscience and Biobehavioral Reviews*. 2006; 30:823–838. [PubMed: 16911826]
- Ryali S, Glover GH, Chang C, Menon V. Development, validation, and comparison of ICA-based gradient artifact reduction algorithms for simultaneous EEG-spiral in/out and echo-planar fMRI recordings. *Neuroimage*. 2009; 48:348–361. [PubMed: 19580873]
- Sijbers J, Michiels I, Verhoye M, Van Audekerke J, Van der Linden A, Van Dyck D. Restoration of MR-induced artifacts in simultaneously recorded MR/EEG data. *Magnetic Resonance Imaging*. 1999; 17:1383–1391. [PubMed: 10576723]
- Sijbers J, Van Audekerke J, Verhoye M, Van der Linden A, Van Dyck D. Reduction of ECG and gradient related artifacts in simultaneously recorded human EEG/MRI data. *Magnetic Resonance Imaging*. 2000; 18:881–886. [PubMed: 11027883]
- Srivastava G, Crottaz-Herbette S, Lau KM, Glover GH, Menon V. ICA-based procedures for removing ballistocardiogram artifacts from EEG data acquired in the MRI scanner. *Neuroimage*. 2005; 24:50–60. [PubMed: 15588596]
- Tong S, Bezerianos A, Paul J, Zhu Y, Thakor N. Removal of ECG interference from the EEG recordings in small animals using independent component analysis. *J Neurosci Methods*. 2001; 108:11–17. [PubMed: 11459613]
- Vanderperren K, De Vos M, Ramautar JR, Novitskiy N, Mennes M, Assecondi S, Vanrumste B, Stiers P, Van den Bergh BRH, Wagemans J, Lagae L, Sunaert S, Van Huffel S. Removal of BCG artifacts from EEG recordings inside the MR scanner: A comparison of methodological and validation-related aspects. *Neuroimage*. 2010; 50:920–934. [PubMed: 20074647]
- Vincent JL, Larson-Prior LJ, Zempel JM, Snyder AZ. Moving GLM ballistocardiogram artifact reduction for EEG acquired simultaneously with fMRI. *Clinical Neurophysiology*. 2007; 118:981–998. [PubMed: 17368972]
- Wan X, Iwata K, Riera J, Kitamura M, Kawashima R. Artifact reduction for simultaneous EEG/fMRI recording: adaptive FIR reduction of imaging artifacts. *Clin Neurophysiol*. 2006; 117:681–692. [PubMed: 16458593]
- Yan WX, Mullinger KJ, Geirsdottir GB, Bowtell R. Physical Modeling of Pulse Artefact Sources in Simultaneous EEG/fMRI. *Human Brain Mapping*. 2010; 31:604–620. [PubMed: 19823981]

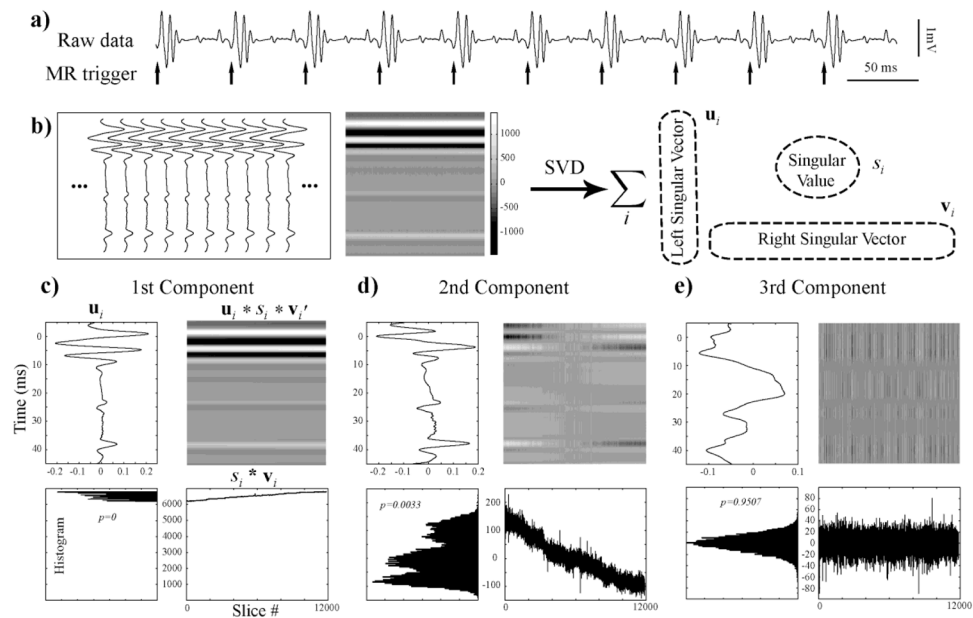


Figure 1.

a) Artifactual SVD component selection for gradient artifact removal is based on raw data recorded from a single channel and triggers sent from the MRI scanner on every slice acquisition. **b)** Segmented raw data arranged into a matrix and then decomposed into orthogonal components by SVD. The first, second and third SVD components for this example dataset are shown in **c)**, **d)** and **e)**. In the insets of **c)**, **d)** and **e)**, the left singular vector is shown in top-left; the right singular vector is shown in bottom-right; the histogram of the right singular vector is shown in bottom-left.

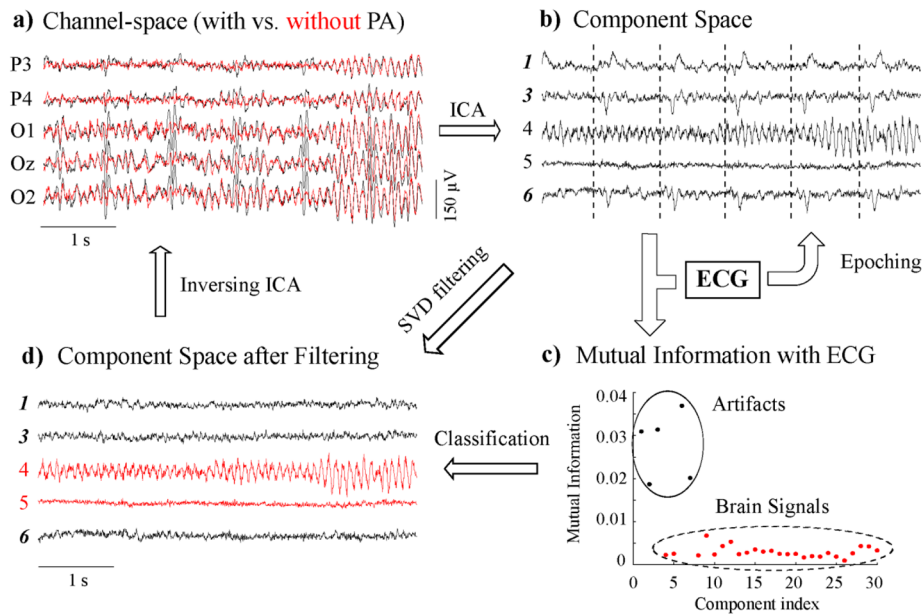


Figure 2. Pulse artifact correction by ICA and SVD filtering. **a)** Multi-channel EEG signals before (in black) and after (in red) pulse artifact correction. **b)** Multi-component time series obtained by applying ICA to the signals recorded from all EEG channels. **c)** Mutual information between every component time course and the ECG. PA-related components are selected from the cluster with high mutual information. **d)** Multi-component time series after applying SVD filtering to the time course of each component. The filtered time series of all non-PA components (in red) are inversely transformed to the original channel space, resulting in the corrected (red) traces in **a)**.

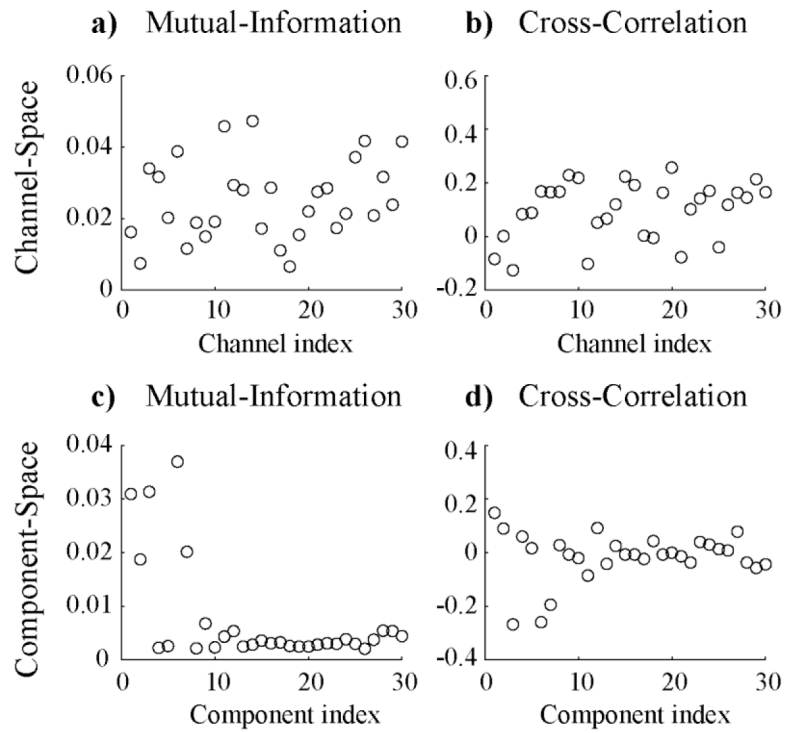


Figure 3. Mutual information (**a, c**) or cross correlation (**b, d**) between channel-wise (**a, b**) or component-wise (**c, d**) time-series signals and ECG for an example EEG dataset.

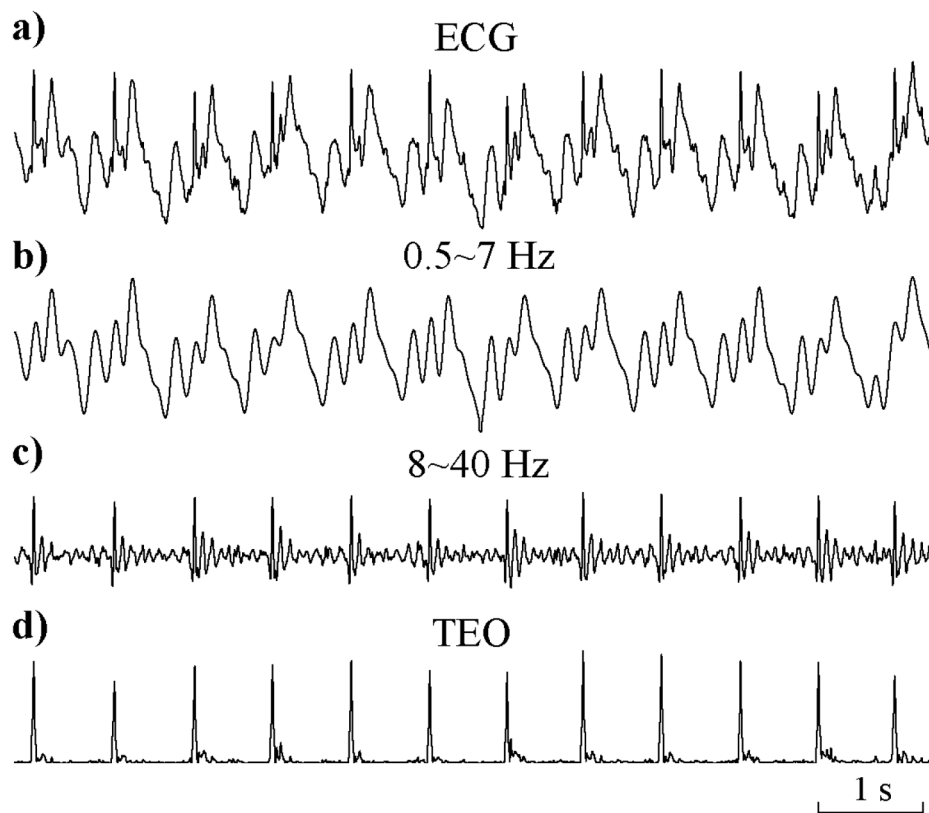


Figure 4. TEO signal generation. **a)** ECG signal. **b)** band-pass filtered ECG signal from 0.5 to 7 Hz. **c)** band-pass filtered ECG signal from 8 to 40 Hz. **d)** TEO signal obtained by applying TEO to the band-pass filtered ECG displayed in **c)**.

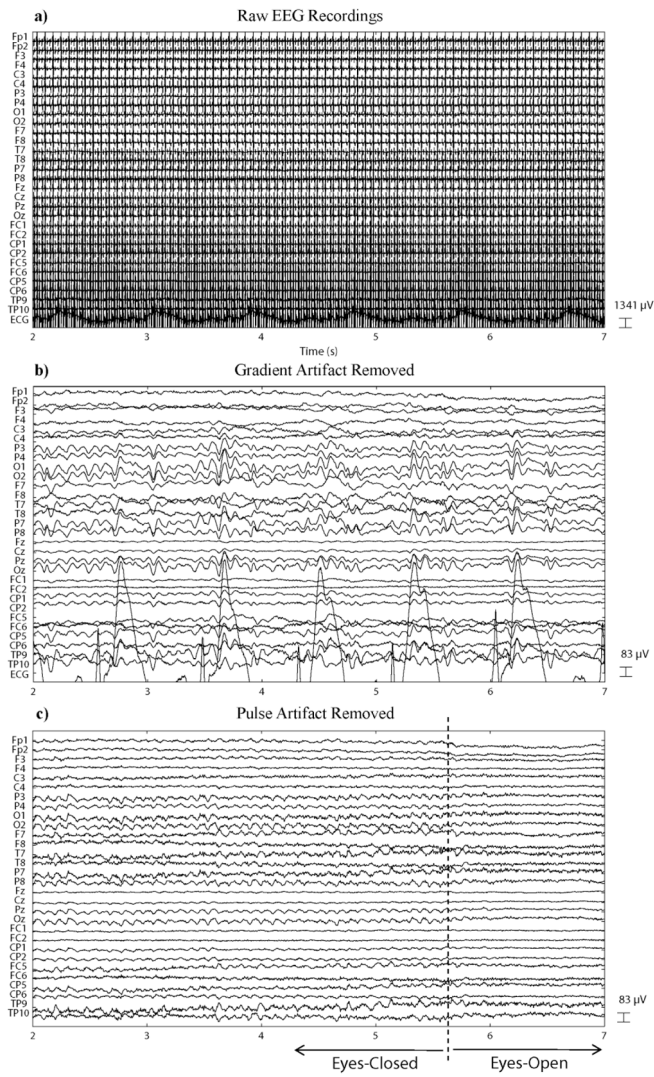


Figure 5. a) Raw time-series data recorded from 30 EEG channels and one ECG channel. b) Signals after removing gradient artifacts. c) Signals after removing both gradient and pulse artifacts. Note the substantially larger scale used in (a).

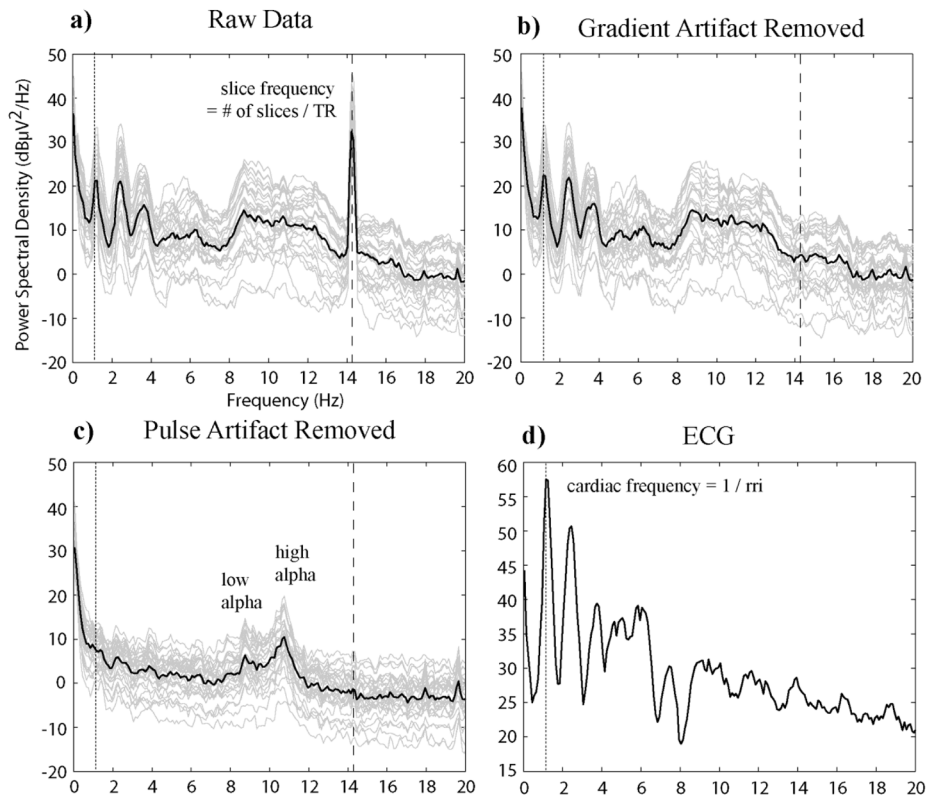


Figure 6. Power spectral density function profiles for raw data (a), the signals after gradient artifact removal (b), the signals after the removal of both gradient and pulse artifacts (c), and the ECG after gradient artifact removal (d).

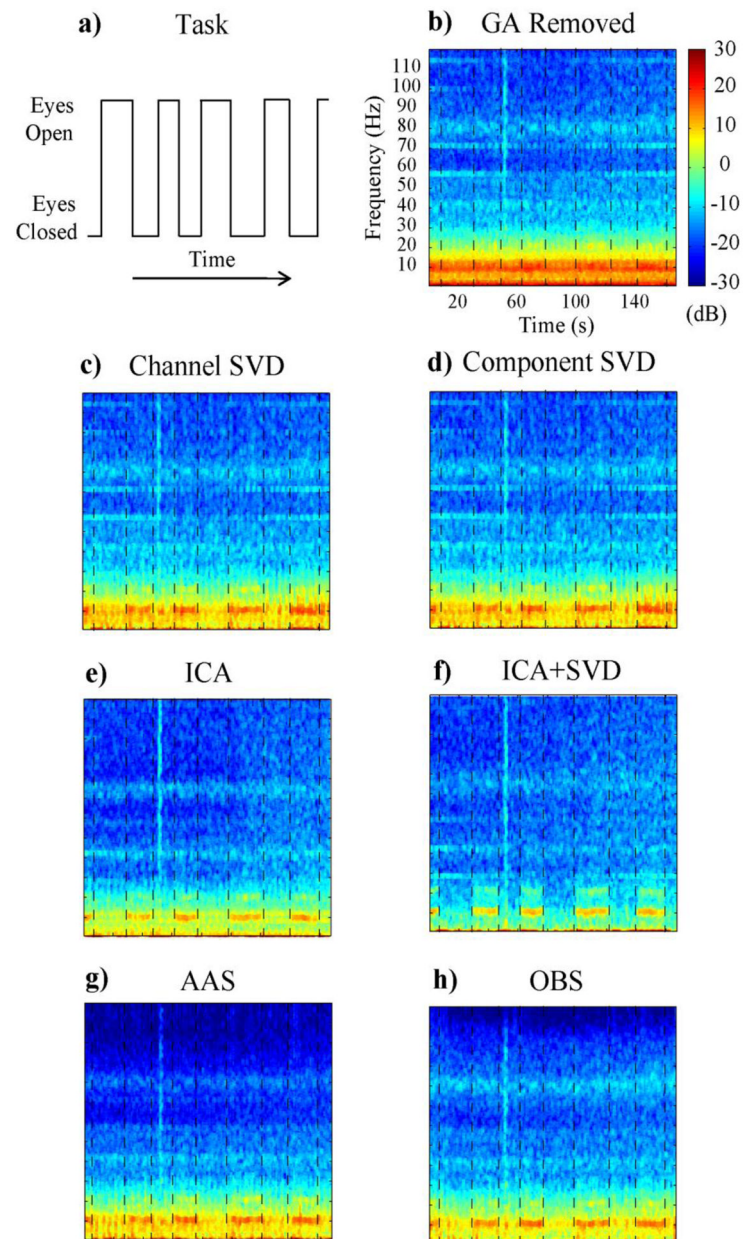


Figure 7.

EEG responses for a self-paced eyes-closed-eyes-open task, illustrated in (a). Single-channel (Oz) spectrograms are shown for the signal contaminated by pulse artifacts (b), the signal corrected by applying the SVD filtering to the channel-wise (c) or component-wise (d) time series, the signal corrected by removing PA-related ICs (e), the signal corrected by both applying the SVD filtering to component time courses and removing PA-related ICs (f, and). The signals corrected using the AAS (g) and OBS (h) methods are also shown.

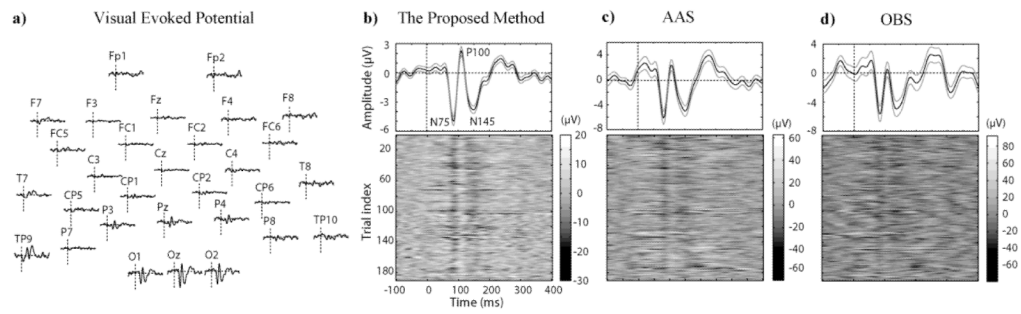
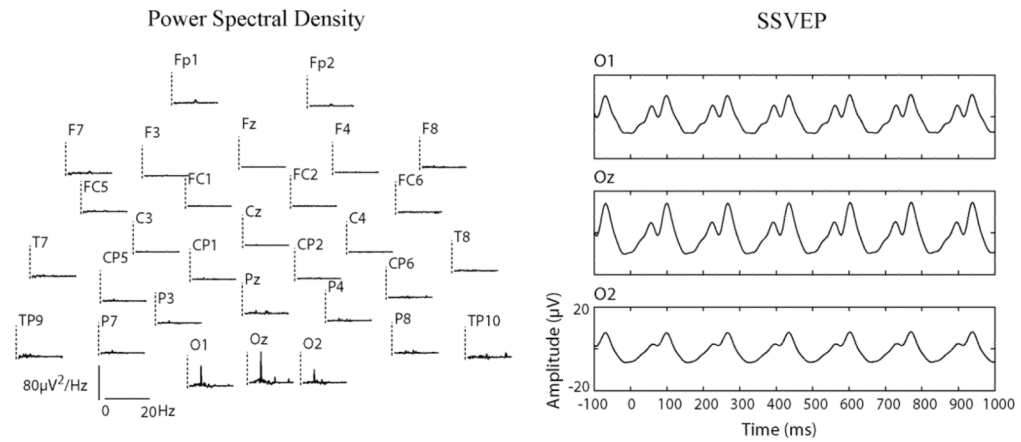


Figure 8.

a) VEP signals from -100 to 400 ms with respect to the stimulus onset. **b)** Mean and single-trial VEP signals after using the proposed method. On the top is the mean VEP signal at Oz (black) with standard errors computed across trials (grey); on the bottom are the electrical responses to individual stimuli. Panes **c)** and **d)** show the VEP signals after using the AAS and OBS methods, respectively.

a) 6Hz visual stimulation



b) 10Hz visual stimulation

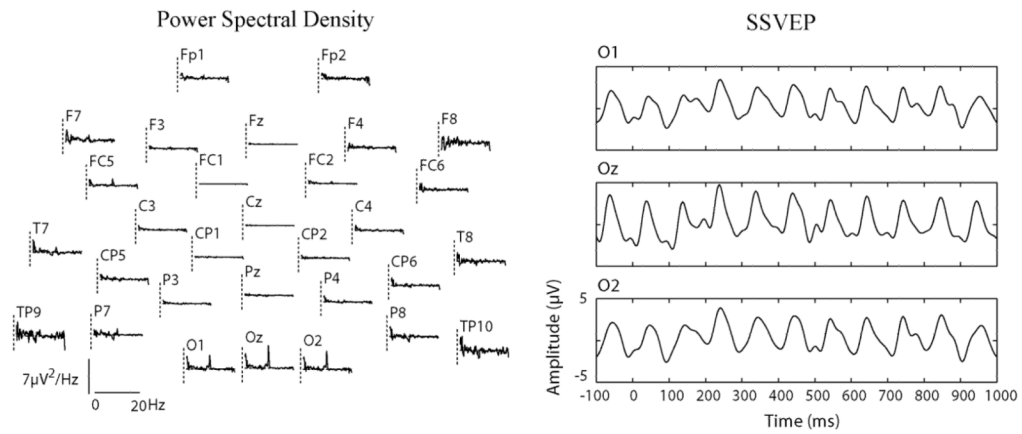
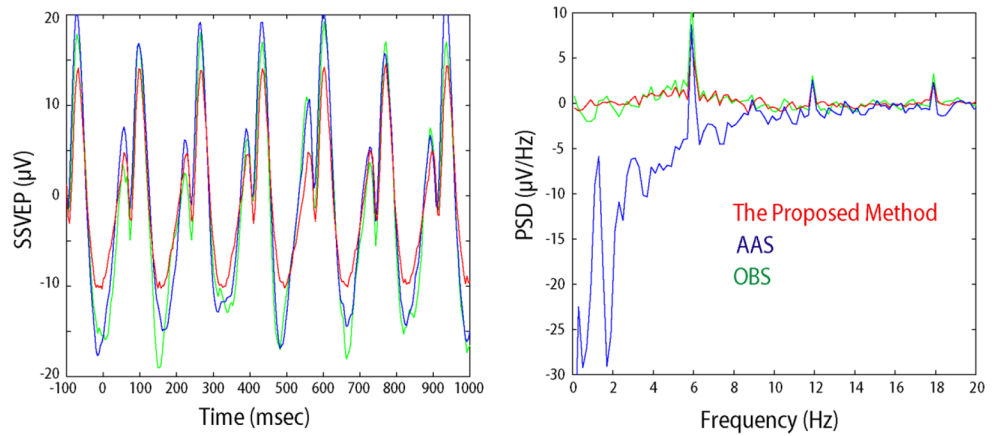


Figure 9. Power spectral density functions (left) and time courses (right) of the SSVEP signals generated by 6Hz (a) and 10Hz (b) visual stimulation. Spectra are displayed for all EEG channels. Time courses are shown only for three occipital channels (O1, Oz and O2).

6 Hz Visual Stimulation

**Figure 10.**

Steady-state visual evoked potentials for the Oz electrode for one of the 6 Hz visual stimulation experiment, represented in time (left) and frequency (right) domain, obtained with three different methods: our method (red), AAS (blue) and OBS (green). Note that the data from the method presented here are identical to the Oz-data shown in Fig. 9a.

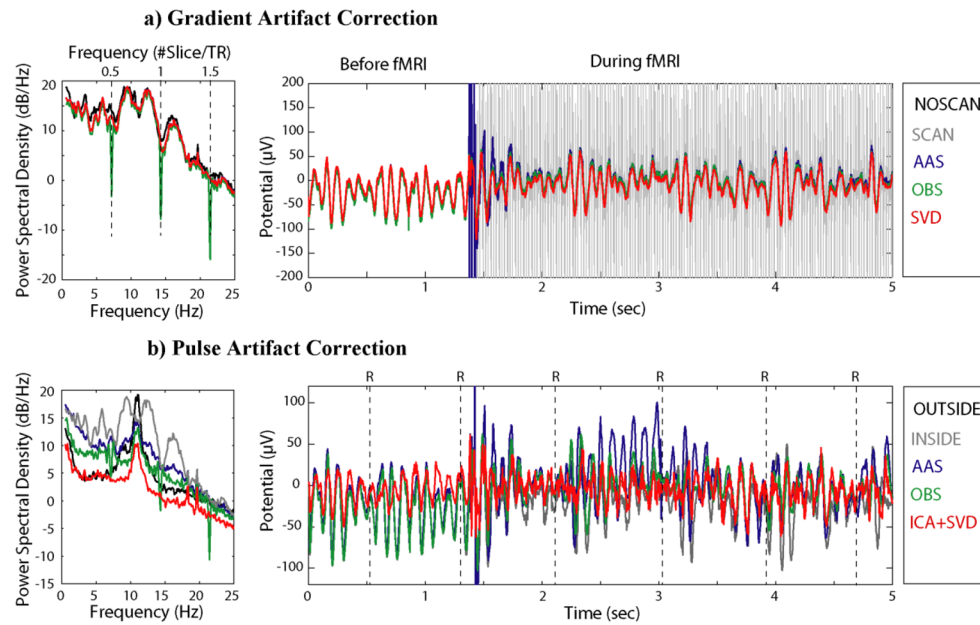


Figure 11.

Comparison between the proposed method and two other existing methods (AAS and OBS) for resting-state EEG. **a)** Spectra (left) and time courses (right) of the EEG signal at Pz corrected for gradient artifacts with the proposed method (red), AAS (blue) and OBS (green) in comparison with the signal recorded without fMRI (black) or with fMRI but without any artifact correction (gray). **b)** Spectra (left) and time courses (right) of the EEG signal at Pz further corrected for pulse artifact with the proposed method (red), AAS (blue) and OBS (green) in comparison with the signal recorded outside the MRI scanner (black) and the signal before any pulse artifact correction (gray).

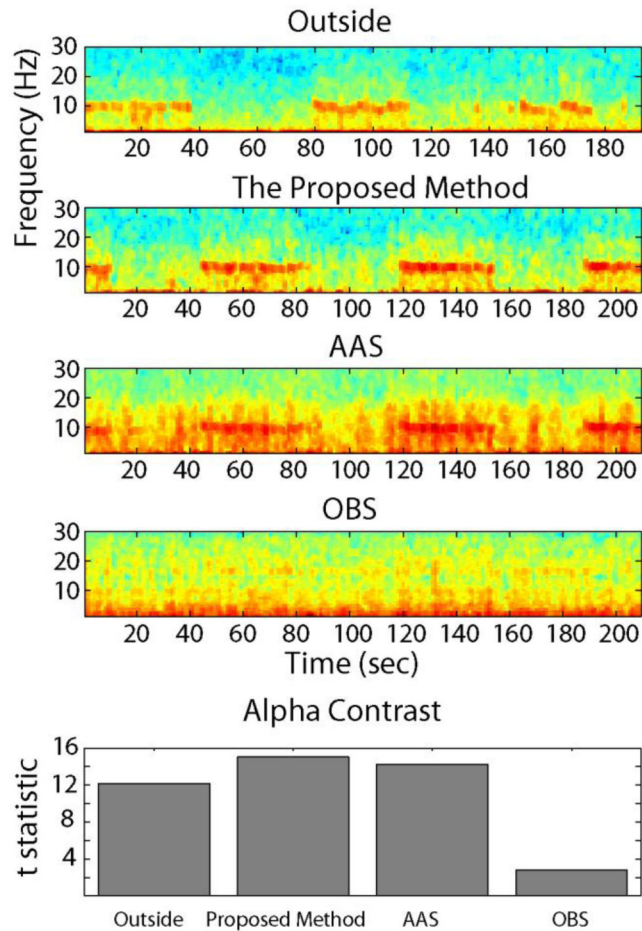


Figure 12.

Performance of the proposed method and two other existing methods (AAS and OBS) for the alpha power modulation induced by opening and closing eyes, in comparison with the data recorded outside the scanner. The first four rows (from top to bottom) are the alpha power modulation at the Oz channel recorded outside, recorded inside and processed with the proposed method, AAS and OBS. The bottom row is the alpha contrast between eyes-closed and eyes-open periods quantified with two-sample t-test.

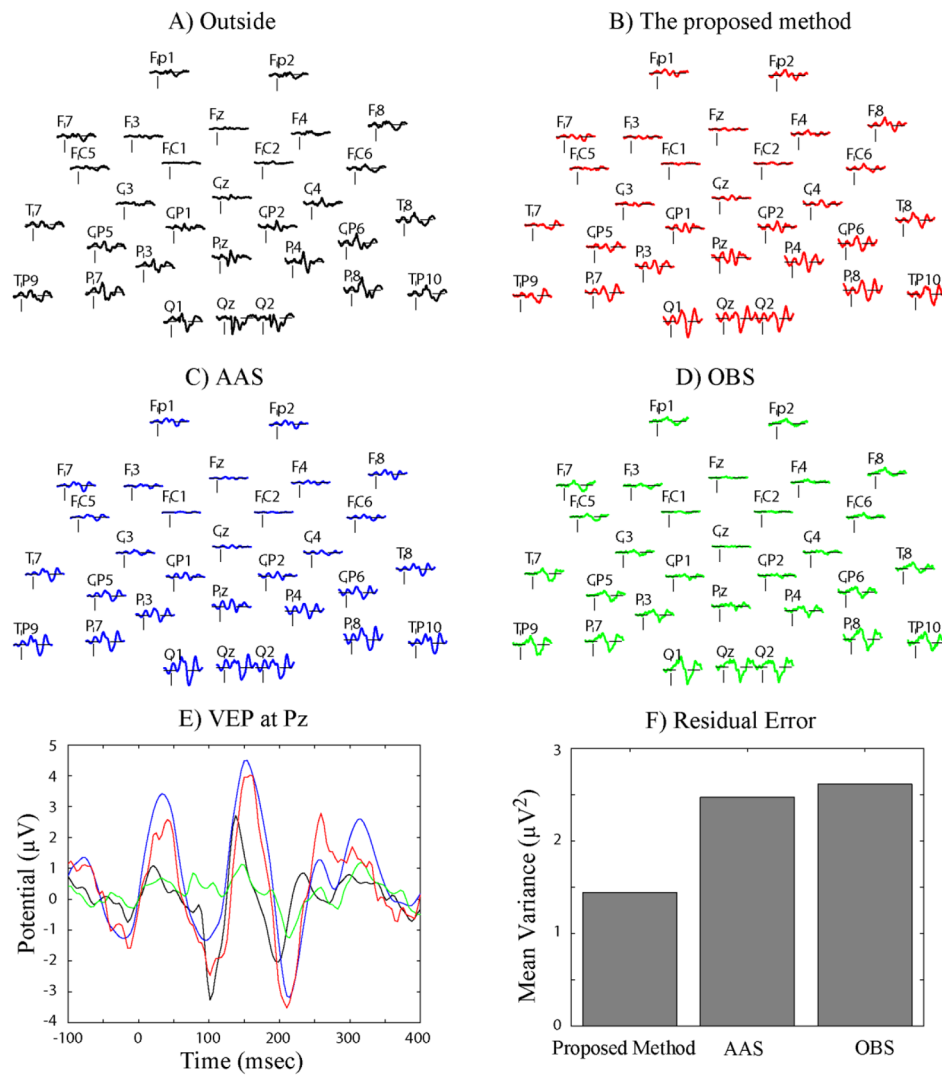


Figure 13.

Assessment of the proposed method and two other existing methods (AAS and OBS) for quality of VEP signals recorded in the scanner in comparison with those recorded outside the scanner. A) VEP recorded outside the scanner, B) VEP recorded inside the scanner on the same volunteer on the same day, obtained with the proposed method, C) the same data as B) processed with AAS, D) the VEP recorded inside the scanner after processing with OBS, E) VEP at a single channel obtained with different methods, compared to that recorded outside the scanner for the same subject, F) residual errors (difference between the VEP recorded outside and inside the scanner) quantified by the mean variance averaged across channels, resulting from the use of different methods.

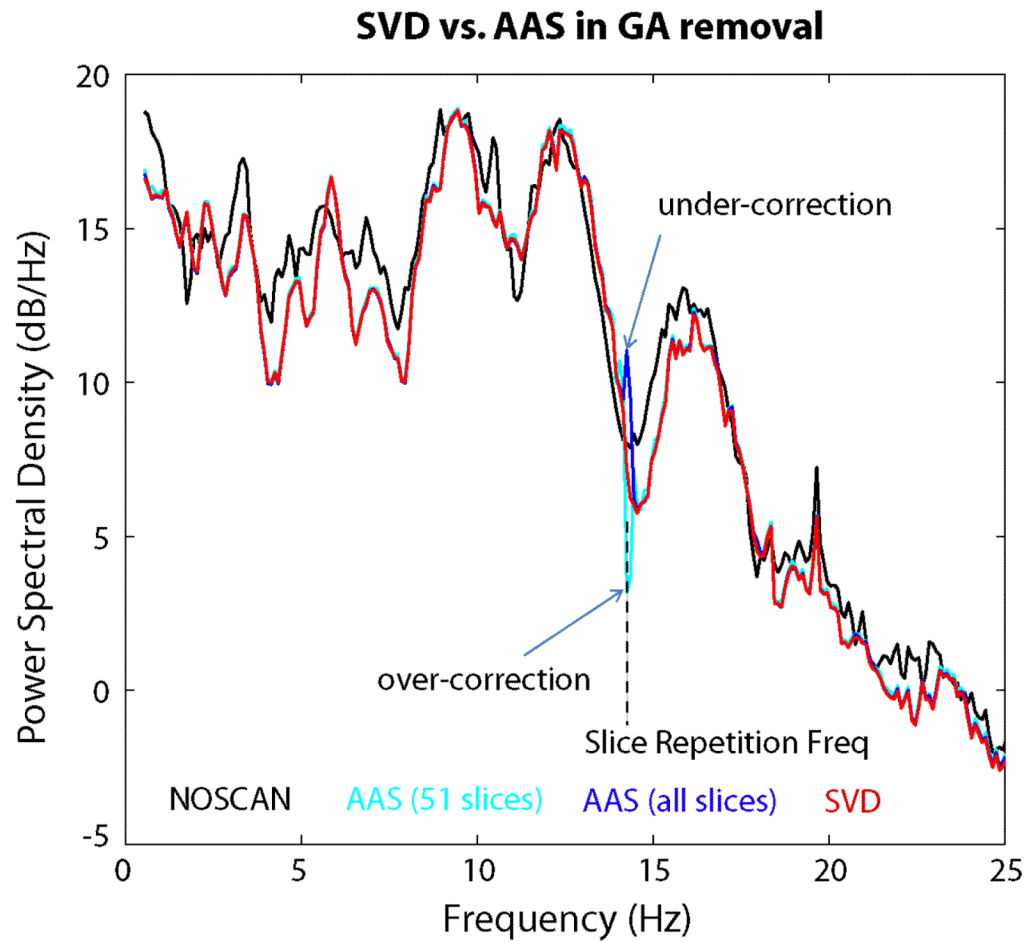


Figure 14. Comparison of the EEG spectra for experiments without (black) and with concurrent fMRI acquisition. The latter data were processed using the proposed method (red) and the AAS method with two different moving windows containing 51 (cyan) or all (blue) slice acquisitions.